Geophysical Research Letters

RESEARCH LETTER

10.1029/2021GL093496

Untangling the Relationship Between AMOC Variability and North Atlantic Upper-Ocean Temperature and Salinity

J. C. H. Chiang[1], **W. Cheng**[2,3], **W. M. Kim**[4], **and S. Kim**[1]

[1]Department of Geography, University of California, Berkeley, CA, USA, [2]Cooperative Institute for Climate, Ocean, and Ecosystem Studies, University of Washington, Seattle, WA, USA, [3]NOAA/Pacific Marine Environmental Laboratory, Seattle, WA, USA, [4]Climate and Global Dynamics Laboratory, National Center for Atmospheric Research, Boulder, CO, USA

Key Points:

- Maximum covariance analysis reveals two modes that separate cause-and-effect between Atlantic meridional overturning circulation (AMOC) and North Atlantic temperature/salinity in a control simulation
- The two modes effectively span the temporal behavior of AMOC variability as represented by the AMOC maximum streamfunction index
- Analysis of simulation with oscillatory and red-noise AMOC regimes indicate that North Atlantic-forced AMOC is suppressed in latter regime

Supporting Information:

Supporting Information may be found in the online version of this article.

Correspondence to:

J. C. H. Chiang,
jch_chiang@berkeley.edu

Citation:

Chiang, J. C. H., Cheng, W., Kim, W. M., & Kim, S. (2021). Untangling the relationship between AMOC variability and North Atlantic upper-ocean temperature and salinity. *Geophysical Research Letters*, *48*, e2021GL093496. https://doi.org/10.1029/2021GL093496

Received 22 MAR 2021
Accepted 3 JUL 2021

Abstract The relationship between Atlantic meridional overturning circulation (AMOC) variability and high-latitude North Atlantic buoyancy changes is complicated by the latter both driving, and responding to, AMOC changes. A maximum covariance analysis applied to a 1,201-year preindustrial control simulation reveals two leading modes that separate these two distinct roles of North Atlantic temperature and salinity as related to AMOC variability. A linear combination of the two modes accounts for most of the variation of a widely used AMOC index. The same analysis applied to another control simulation known to possess two distinct regimes of AMOC variability—oscillatory and red-noise—suggests that the North Atlantic buoyancy-forced AMOC variability is present in both regimes but is weaker in the latter, and moreover there is pronounced multidecadal/centennial AMOC behavior in the latter regime that is unrelated to North Atlantic buoyancy forcing.

Plain Language Summary Atlantic meridional overturning circulation (AMOC) variations cause significant changes to the global climate. High-latitude North Atlantic temperature and salinity variations modify the AMOC through changing the buoyancy of the upper ocean. However, this identification is complicated by the reverse relationship, that North Atlantic temperature and salinity changes with AMOC. When we apply maximum covariance analysis—a spatiotemporal analysis designed to find coupled patterns between two climate fields—to a preindustrial control simulation of a fully coupled climate model, it extracts the two coupling relationships. Moreover, the combination of these two behaviors is sufficient to characterize the AMOC variations. When we apply the same analysis method to another control simulation exhibiting two regimes of AMOC variability—oscillatory and red-noise—it reveals that the red-noise regime has a marked reduction to the AMOC variability resulting from North Atlantic buoyancy forcing, and a corresponding increase in multidecadal/centennial AMOC variations of undetermined origin.

1. Introduction

This study addresses the interconnected relationship between upper-ocean temperature and salinity in the high-latitude North Atlantic and the variability of the Atlantic meridional overturning circulation (AMOC) on decadal and longer timescales. A number of studies attribute changes to upper-ocean buoyancy anomalies in the high-latitude North Atlantic to drive AMOC variations, the former originating through atmospheric forcing directly on deepwater formation regions (e.g., Danabasoglu, 2008; Delworth et al., 1993; Kim et al., 2020), or mediated to the western boundary though advection or Rossby wave propagation (e.g., Buckley et al., 2012). Idealized simulations where a pulse buoyancy forcing is applied to the high-latitude North Atlantic supports this interpretation (Kim et al., 2020; J. Zhang & Zhang, 2015). Many studies also argue for the reverse coupling, that the ocean heat flux convergence caused by AMOC variability drives upper-ocean temperature anomalies in the high-latitude North Atlantic (e.g., Häkkinen, 1999; J. Zhang & Zhang, 2015; R. Zhang, 2008). However, for internal AMOC variations in climate model simulations, co-mingling of the two processes means that the cause-and-effect relationship is difficult to establish.

Untangling these directional relationships is key to understanding AMOC variability (Buckley & Marshall, 2016). Some have argued that the ocean dynamical response in the high-latitude North Atlantic to the

AMOC variation induces a delayed feedback that alters the behavior of the AMOC, including its persistence (Kwon & Frankignoul, 2012) or timescale of variation (Dong & Sutton, 2005; Griffies & Tziperman, 1995; Kwon & Frankignoul, 2014). In contrast, others have argued that the AMOC variation is a passive response to buoyancy anomalies in the high-latitude North Atlantic (e.g., Buckley et al., 2012). Untangling these relationships also reveals the nature of the forced AMOC response to a warming climate: Tandon and Kushner (2015) found in historical model simulations that an unforced AMOC increase lead to North Atlantic sea surface temperature (SST) warming, whereas a forced warming of North Atlantic SST leads to an AMOC weakening.

There exists an objective spatiotemporal analysis technique—maximum covariance analysis (MCA; Bretherton et al., 1992)—designed to extract coupled patterns between two climate fields, such as the problem described above. A lagged MCA has previously been used to reveal the two-way response of the North Atlantic atmosphere with AMOC variability (Gastineau & Frankignoul, 2012). However, MCA has not been previously applied to relate AMOC variations to North Atlantic upper-ocean temperature and salinity. Also, studies linking AMOC changes to underlying drivers or responses typically assume an index of AMOC strength to represent the totality of AMOC variations, for example, the first EOF of the meridional overturning circulation (MOC) streamfunction, or the maximum value of the MOC streamfunction within the North Atlantic. The choice of index is somewhat subjective, and moreover does not allow for diversity in the spatiotemporal structure of AMOC variability. A MCA approach, on the other hand, makes no prior assumptions about the structure of AMOC variations.

In the following, we apply MCA to a control simulation of a fully coupled model to objectively extract coupled spatial patterns between AMOC and high-latitude North Atlantic upper-ocean temperature and salinity. We also apply the MCA to a control simulation of another model that exhibits two regimes of AMOC behavior, oscillatory and red-noise, to examine what the method reveals about the nature of the two regimes.

2. Materials and Methods

We use years 1,000–2,200 of a preindustrial (1,850) control run of the Community Earth System Model version 1.2 (CESM1) at 1° horizontal resolution as described in Kay et al. (2015) (years 1–1,000 shows a downward trend in the AMOC strength). We also use a T85 simulation of the Community Climate System Model version 3 (hereafter CCSM T85) that has been extensively analyzed for AMOC specifically its regime shift (Danabasoglu, 2008, Danabasoglu et al., 2012; Kwon & Frankignoul 2012, 2014). We also use a set of idealized CESM1 simulations where a pulse buoyancy forcing designed to mimic the effect of a boreal winter (December–March) North Atlantic Oscillation (NAO) event was applied to the Labrador Sea to examine its effect on the AMOC. The runs are the same as in Kim et al. (2020). A heat flux anomaly was applied over 10 years to the Labrador Sea domain 50–64°N and 45–61°W representative of a NAO event; a set of 10 ensemble members were run with positive values of the anomaly, and another 10 with negative values. The reader is referred to Kim et al. (2020) for simulation details.

MCA is used to extract coupled patterns relating AMOC to North Atlantic upper-ocean temperature and salinity, following Bretherton et al. (1992). For the left field, we use the annual mean MOC streamfunction anomalies in the Atlantic. That data are first interpolated (using bilinear interpolation) onto an equally spaced latitude and depth grid, from 33.5°S to 65.5°N in intervals of 1°, and from 50 to 4,950 m in steps of 100 m. The data are then detrended and light temporal smoothing (5-year running mean) is applied to remove the interannual variation. For the right field, we use the annual mean temperature and salinity anomalies averaged over the top 1,000 m for the North Atlantic north of 40°N; the data are left on the native ocean model horizontal grid. The temperature and salinity anomalies are converted to their density equivalents, multiplied by the square root of the grid area, and the resulting data combined to form a single field. A cross-covariance matrix is formed using the left and right fields, and a singular value decomposition is applied to solve for the MCA modes. The first two modes account for over 90% of the cumulative squared covariance fraction (Figure S1); our analysis focuses on these two modes. In subsequent analysis, the spatial patterns shown are homogeneous regression maps, calculated by regressing the field of interest onto the normalized expansion coefficient. Regression slopes are only plotted if the associated correlation coefficient

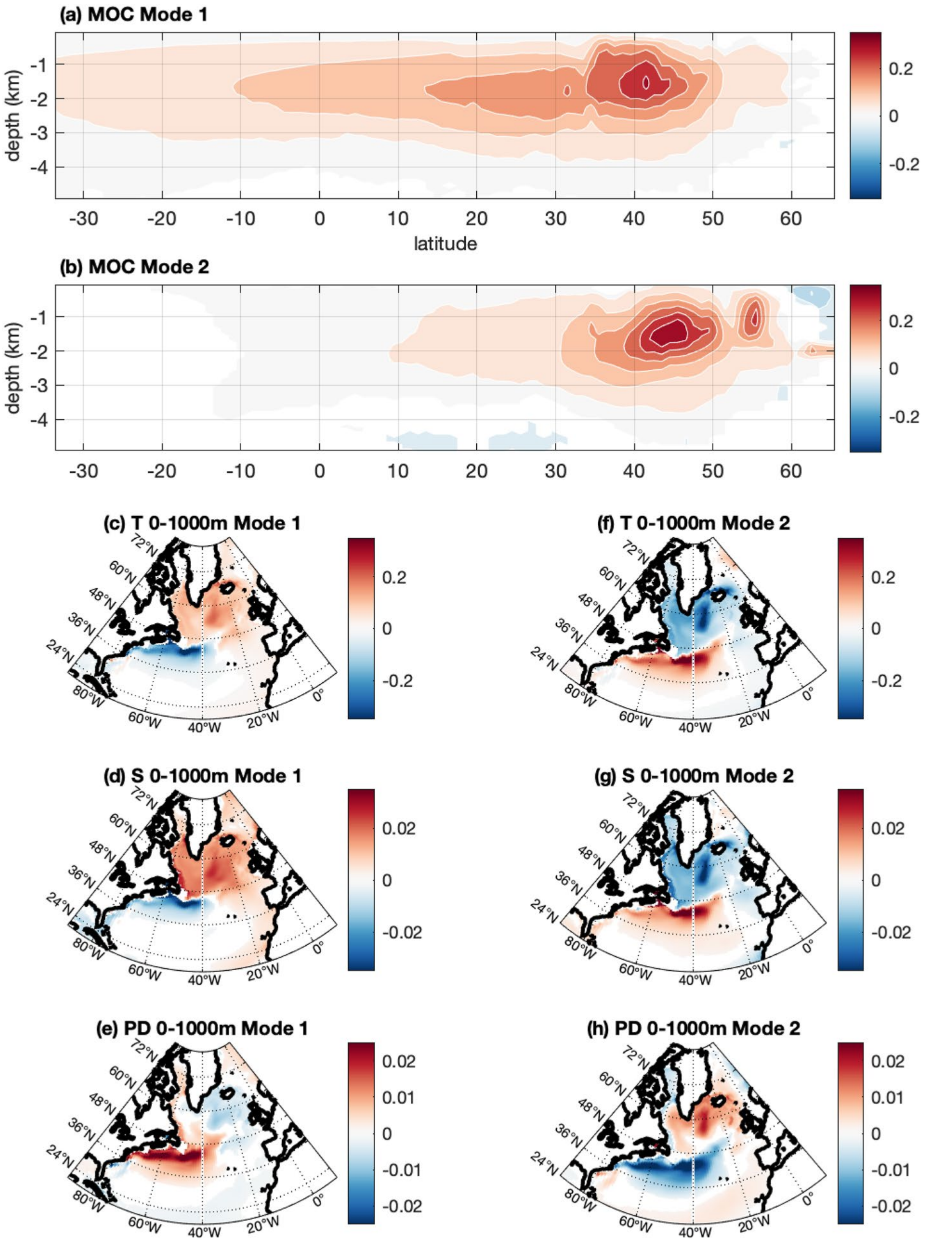

Figure 1. Maximum covariance analysis on Community Earth System Model version 1.2. (a) Homogeneous regression map onto mode 1 meridional overturning circulation (MOC) expansion coefficients. (b) Same as (a), for mode 2. (c–e) Regression maps of 0–1,000 m averaged (c) temperature, (d) salinity, and (e) potential density onto mode 1 temperature/salinity (T/S) expansion coefficients. (f–h) Same as (c–e), for mode 2. Values are shown only where the correlation is significant ($p < 0.05$).

is significantly different from zero. Significance of correlations is assessed using the t-statistic and with the effective sample size calculated using Equation 2 of Ebisuzaki (1997).

3. MCA Analysis on CESM1

Figure 1a and Figure S2a show the MOC spatial pattern and expansion coefficients associated with mode 1, respectively. It is characterized by an interhemispheric AMOC increase, associated with warmer and saltier waters in the high-latitude North Atlantic by the Irminger and Labrador seas (Figures 1c and 1d). The associated potential density changes (Figure 1e) are largely negative but small, indicating compensation between the temperature and salinity changes. The variation for both the MOC and temperature/salinity (hereafter T/S) expansion coefficients are dominated by lower frequencies between 25- and 250-year period (Figures S2c and S2d, blue lines). Lag correlation between the MOC and T/S expansion coefficients show that the MOC expansion coefficients lead that for T/S by 1–3 years (Figure S2e). They suggest that the temperature and salinity patterns seen in Figures 1c and 1d are a consequence of the AMOC strengthening.

Figure 1b and Figure S2b show the MOC spatial pattern and expansion coefficients associated with mode 2, respectively. It is characterized by an AMOC increase limited to the mid and high-latitude North Atlantic and associated with colder and fresher upper-ocean waters there (Figures 1f and 1g) and potential density increase near the Irminger and Labrador seas (Figure 1h). The variation for the MOC expansion coefficients peak between 20- and 50-year period (Figure S2c, red line), whereas the T/S expansion coefficients peak possess a broader spectrum (Figure S2d, red line). For the MOC (left) expansion coefficients, mode 1 has generally lower frequencies but there is an overlap between mode 1 and mode 2 between around 0.025/yr and 0.04/yr (Figure S2c). Lag correlation between the MOC and T/S expansion coefficients show that the latter leads the former by 1 year (Figure S2f). The results suggest that this mode represents the AMOC responding to increase in North Atlantic upper-ocean density from cooler ocean temperatures.

As a check to see whether temperature or salinity dominates the MCA result, the MCA was repeated using each field individually. In each case, the MCA mode 1 and 2 spatial patterns closely resembled those for the MCA with both temperature and salinity (figure not shown). Moreover, the correlation between the mode 1 MOC expansion coefficients for the MCA with only temperature or salinity, with the full MCA, is high ($r > 0.94$ in both cases), and similarly for mode 2. Thus, both temperature and salinity contribute to the MCA result.

To check the temporal relationships inferred from the MCA analysis, we repeated the MCA but with a temporal shift applied to the T/S field relative to the MOC field (Czaja & Frankignoul, 1999; Gastineau & Frankignoul, 2012). The assumption is that the squared covariance explained for the mode of interest will be maximized when the lag reflects the physical coupling extracted. The results are consistent with the lead/lag relationship between MOC and T/S for modes 1 and 2 stated above. The squared covariance fraction for mode 1 is maximized when MOC leads T/S by 5 years (Figure S3, blue bars). The MOC expansion coefficients at this lag correlate with mode 1 for our original MCA (zero lag) at $r = 0.976$, meaning that they represent the same physical process. For mode 2, the squared covariance fraction maximizes when MOC lags T/S by 1 year, and the left expansion coefficients for this mode at this lag correlates with mode 2 for our original MCA (zero lag) at $r = 0.984$. We revert to the original (i.e., unlagged) MCA modes for the subsequent discussion.

Modes 1 and 2 are curious as the temperature and salinity changes appear to be diametrically opposite: mode 1 associates an AMOC increase with a warmer and saltier high-latitude North Atlantic, whereas mode 2 associates an AMOC increase (albeit at high latitudes) with a colder and fresher high-latitude North Atlantic. We interpret the two modes to represent two different stages of the AMOC variation: mode 2 shows the initial response of the AMOC to colder and denser high-latitude North Atlantic waters, whereas mode 1 shows the subsequent evolution where the AMOC strengthening extends southwards, and the resulting ocean circulation change leads to a warmer and saltier high-latitude North Atlantic.

Two pieces of evidence support this interpretation. First, a lag correlation between the MOC expansion coefficients for the two modes (Figure 2a) shows that they are significantly correlated, and that peak correlation ($r = 0.64$) occurs when mode 2 leads mode 1 by 2–3 years; in other words, the high-latitude MOC increase (Figure 1b) precedes the interhemispheric MOC increase (Figure 1a). Second, an idealized simulation with an NAO-like density perturbation in the North Atlantic using the same CESM1 model (Kim et al., 2020; see Section 2) shows the evolution of the MOC from one restricted to the high-latitude North Atlantic in the first few years, to a more interhemispheric pattern in the second decade of its evolution (Figure 2b–2d). The initial MOC perturbation resembles the MCA mode 2 pattern (Figure 1b), whereas the later MOC perturbation resembles the MCA mode 1 pattern (Figure 1a). A similar MOC evolution to a pulse-like NAO buoyancy forcing is seen in the GFDL CM2.1 (Delworth & Zeng, 2016). This interpretation is also consistent with the evolution of AMOC anomalies found in many previous studies (e.g., Biastoch et al., 2008; Deshayes & Frankignoul, 2008; Kwon & Frankignoul, 2014; J. Zhang & Zhang, 2015).

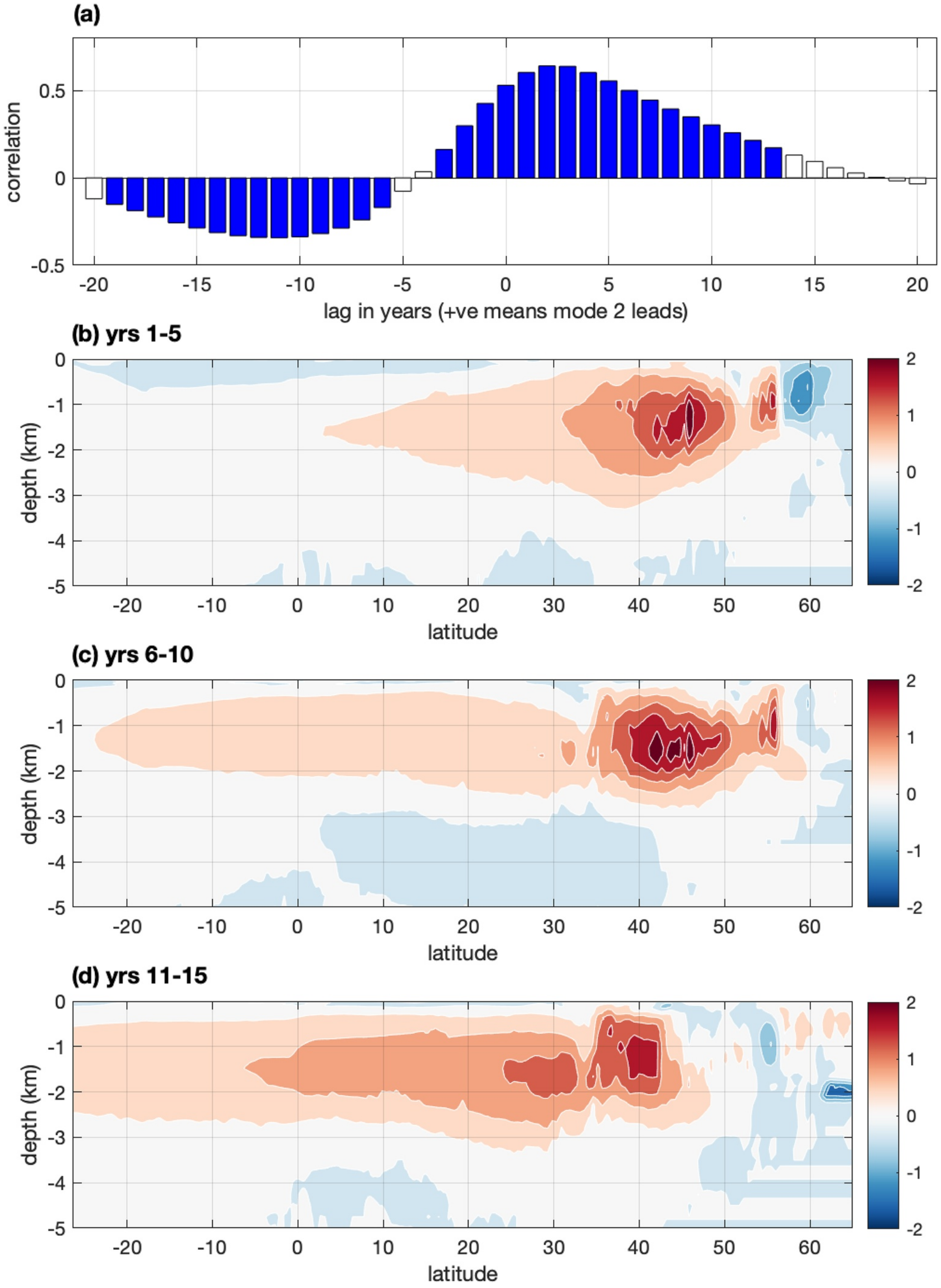

Figure 2. (a) Lag correlation between mode 1 and 2 meridional overturning circulation (MOC) expansion coefficients. Significant correlations ($p < 0.05$) are indicated by filled bars. (b–d) Community Earth System Model version 1.2 transient Atlantic meridional overturning circulation response to an imposed pulse buoyancy flux anomaly over the Labrador Sea. The years indicated correspond to the average of years after onset of the forcing. Contour interval is 0.4 Sv.

The MCA thus decomposes the AMOC variability into two modes, each with its own spatial pattern and temporal behavior. How do they relate to traditional indices of AMOC variability? We compare the MOC expansion coefficients to a standard index for the AMOC, namely the maximum AMOC streamfunction value (below 500 m depth) at a given latitude. Using this AMOC index at 47.5°N, we find that a multivariate linear regression using the modes 1 and 2 MOC expansion coefficients (over the entire 1,201 years) as

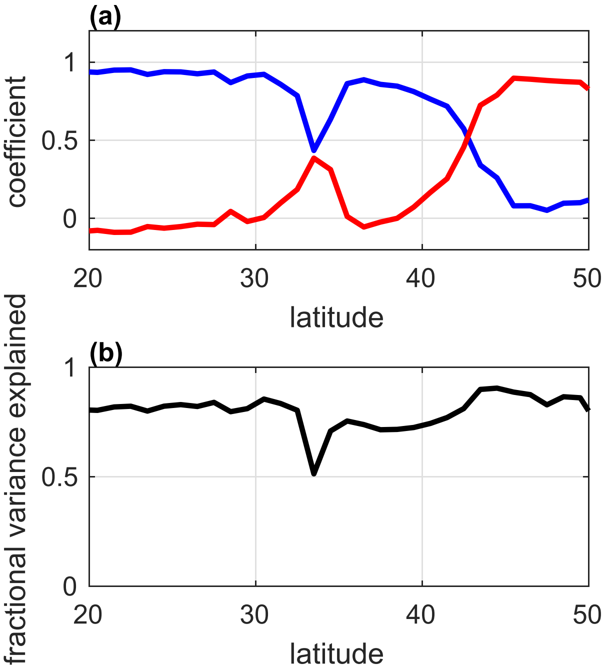

Figure 3. Multivariate regression of mode 1 and 2 meridional overturning circulation expansion coefficients with the Atlantic meridional overturning circulation (AMOC) maximum streamfunction at the given latitude, over the entire 1,201 years. (a) Regression coefficient as a function of latitude for mode 1 (blue) and 2 (red). (b) Fractional variance explained of the AMOC maximum streamfunction by the best-fit linear sum of modes 1 and 2.

predictors provides a good fit, but with most of the fit coming from mode 2 (the high-latitude AMOC pattern) (Figure S4, left panels). On the other hand, for the AMOC index at 37.5°N, the linear combination again provides a good fit but with most of it coming from mode 1, the interhemispheric MOC pattern (Figure S4, right panels). The same comparison for each latitude between 20 and 50°N (Figure 3) reveals that the two MOC expansion coefficients are consistently able to account for most of the variance (>70%) of the AMOC index except for a narrow band between 33 and 34°N (Figure 3b). Mode 2 essentially represents the AMOC maximum streamfunction value at higher latitudes, and mode 1 represents the AMOC maximum streamfunction value for lower latitudes, with 42.5°N being the threshold latitude (Figure 3a). Thus, the two MCA modes encompasses the span of behaviors represented by the AMOC maximum streamfunction index at almost all latitudes of interest between 20 and 50°N. We speculate that the poor fit between 33 and 34°N arises because the MCA analysis does not capture wind-driven MOC variations that contribute substantially to AMOC variation in the midlatitudes (Biastoch et al., 2008; Larson et al., 2020).

4. Analysis of the CCSM3 T85 AMOC Regime Shift

We apply the MCA decomposition to a 699-year CCSM3 T85 simulation that has previously been shown to exhibit two distinct regimes of AMOC variability: an oscillatory regime with pronounced quasi-periodic behavior of ~20 years over years 150–399 (hereafter regime I), and a multidecadal/centennial red-noise like behavior over years 450–699 (hereafter regime II) (Danabasoglu et al., 2012; Kwon & Frankignoul, 2014) (Figure S5). We explore whether the MCA method reveals useful information about the nature of the two regimes. Applying the MCA analysis over years 150–699 reveals that the first two modes dominate, possessing properties qualitatively like the MCA modes 1 and 2 derived for the CESM1 respectively (Figures S6 and S7). As a check, we repeated the MCA for each regime separately; for each instance, the modes 1and 2 obtained possess similar properties to that for the MCA analysis over years 150–699 (not shown).

The regime change in the AMOC is expressed differently in the two modes. Mode 1 is expressed as a timescale change, from quasi-periodic behavior in regime 1 to a pronounced multidecadal/centennial variation in regime 2 (Figure 4a, blue line); this difference is also expressed in the power spectrum for mode 1 MOC expansion coefficients for each regime (Figures S6c and S6d, blue lines). The amplitude of variation of mode 1 is comparably large in both regimes. On the other hand, the regime change in mode 2 is expressed primarily in terms of amplitude, with regime I showing a larger amplitude of variation (Figure 4a and Figures S6c and S6d, red line). Regime II is also more irregular and less periodic than regime I, as inferred from the power spectrum for mode 2 MOC expansion coefficients for each regime (Figures S6c and S6d, red line).

The temporal relationship between modes 1 and 2 also appears to differ between the two regimes. In regime I, the MOC expansion coefficients for mode 2 is correlated to that for mode 1 at $r = 0.71$ with a 4-year lag (mode 1 lags mode 2); this is qualitatively like the relationship seen in the CESM1 (Figure 2a). On the other hand, for regime II, mode 2 is not as strongly correlated with mode 1: the best lead/lag relationship is $r = 0.45$ with a 3-year lag. However, a stronger lead/lag relationship between the two MCA modes for regime II is recovered if we consider only the shorter timescale variations corresponding to the oscillatory behavior. We use ensemble empirical mode decomposition (EEMD; Huang et al., 1998; Wu & Huang, 2009) to filter the MCA expansion coefficients into shorter decadal (periods less than ~64 years) and longer multidecadal/centennial timescales, by using the sum of EEMD intrinsic mode functions (IMFs) 1–4 for the former and EEMD IMFs 5–10 for the latter (Figures 4b and 4c, respectively) (see Section S2 for details). When we repeat the lag correlation but for decadal timescale variations, for regime I, we get $r = 0.77$ for when MCA mode 2 leads mode 1 by 4 years. For regime II, we get $r = 0.61$ when mode 2 leads mode 1 by 3 years (Figure 4b);

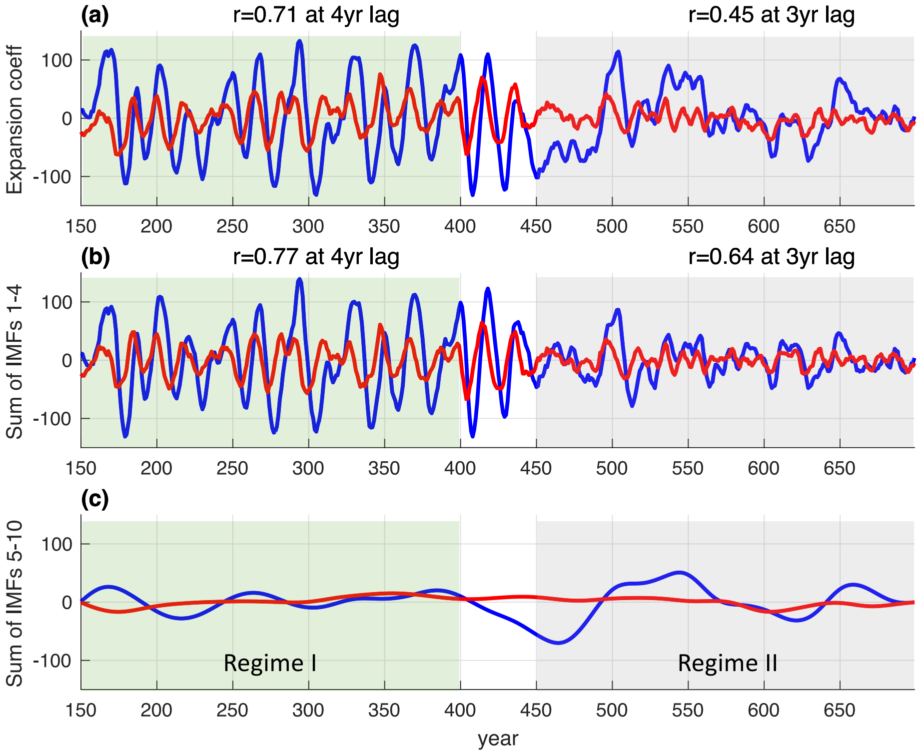

Figure 4. Maximum covariance analysis on Community Climate System Model T85. (a) Meridional overturning circulation expansion coefficients. (b and c) Expansion coefficients filtered for (b) shorter (sum of ensemble empirical mode decomposition intrinsic mode functions [IMFs] 1–4) and (c) longer timescales (sum of IMFs 5–10). Mode 1 is in blue, and 2 in red. Indicated in (a) and (b) are the maximum lead/lag correlation between mode 1 and 2 for each regime, with mode 1 lagging mode 2 by the years indicated.

in other words, we recover the relationship between mode 2 and 1 for these timescales. For the longer multidecadal/centennial timescales, mode 2 has little to no longer-term variation to speak of, and the two modes are clearly unrelated (Figure 4c). This suggests that the longer timescale interhemispheric AMOC behavior has origins independent of high-latitude North Atlantic buoyancy forcing.

We conclude that the high-latitude North Atlantic buoyancy driving of AMOC variability (mode 2) is present in both regimes, albeit weaker in the latter. Kwon and Frankignoul (2014) notes that there is increased densification of the deep ocean (2,000–3,000 m) in regime II relative to regime I, and this may be the reason why regime II has a more muted variation because of the presence of a more stable vertical stratification. On the other hand, the multidecadal/centennial timescale AMOC variability resides almost exclusively in the interhemispheric AMOC response (mode 1) and is strongly expressed in regime II but not regime I (Figure 4c).

5. Summary and Discussion

We examine the relationship between AMOC variability with high-latitude upper-ocean North Atlantic temperature and salinity using a MCA designed to extract coupled modes of variability between the two climate fields. The first two modes explain over 90% of the cumulative squared covariance fraction. Mode 1 possesses an interhemispheric increase in AMOC coupled to a warmer and saltier North Atlantic, and with the MOC expansion coefficients leading the T/S expansion coefficients by 2–3 years. Mode 2 possesses a high-latitude North Atlantic AMOC increase coupled to a colder and fresher high-latitude North Atlantic, qualitatively opposite to mode 1. The two modes represent different phases of AMOC variability driven by buoyancy forcing in the high-latitude North Atlantic: colder SSTs in the high-latitude North Atlantic increases the high-latitude AMOC, which then evolves into an interhemispheric AMOC increase. The resulting AMOC increase leads to ocean circulation changes that bring warmer and saltier upper-ocean water to the high-latitude North Atlantic. This mechanism for AMOC variation has been noted before (e.g., Kwon & Frankignoul, 2014), but the novelty of our result is that the MCA objectively extracts the two distinct couplings.

Our analysis of the two previously identified AMOC regimes—oscillatory and red-noise—of the CCSM3 T85 simulation (Danabasoglu et al., 2012; Kwon & Frankignoul, 2014) suggests that the North Atlantic buoyancy-driven AMOC variability operates at shorter decadal timescales and for both regimes, albeit suppressed in the latter. Moreover, the longer multidecadal/centennial AMOC variability is expressed only in the interhemispheric AMOC (mode 1) and is especially pronounced in the red-noise regime. We conclude that the two regimes arise because (a) the North Atlantic buoyancy-forced AMOC variation is suppressed in the red-noise regime, and (b) the multidecadal/centennial interhemispheric AMOC variation, unrelated to North Atlantic buoyancy forcing, is especially pronounced in the red-noise regime.

Our inferred mechanism for AMOC decadal variability suggests a delayed negative feedback, since a colder high-latitude North Atlantic that starts off the AMOC perturbation ultimately leads to warmer conditions there several years later. A similar feedback was suggested by Kwon and Frankignoul (2014) to explain the 20-year oscillation in regime I of the CCSM3 T85. Why the oscillation manifests itself more strongly in regime I remains an open question, though our analysis suggests that high-latitude North Atlantic buoyancy forcing is less able to excite an AMOC response in regime II, possibly because of the increased vertical stability. Idealized simulations that examine the transient AMOC response to density perturbations under different mean vertical stratification may shed light on this question.

Data Availability Statement

No new data were generated for this work. The CESM1 preindustrial simulation is available at doi:10.5065/d6j101d1 (Kay & Deser, 2016). The CCSM T85 simulation is available from the Climate Data Gateway at the National Center for Atmospheric Research (https://www.earthsystemgrid.org), simulation b30.009. We also utilized Matlab scripts developed by Daniel Vimont (https://www.aos.wisc.edu/∼dvimont/matlab).

Acknowledgments
The authors thank Young-Oh Kwon for providing the MOC streamfunction for the CCSM T85, and Steve Yeager, Gohkan Danabasoglu, Wilber Weijer, and Jiaxu Zhang for useful discussions. This research is supported by the National Oceanic and Atmospheric Administration Climate Program Office under Climate Variability and Predictability Program grants NA16OAR4310169, NA16OAR4310170, NA16OAR4310171; the Regional and Global Climate Modeling Program (RGCM) of the U.S. Department of Energy's (DOE) Office of Science (BER) through support of the HiLAT project, and by the National Science Foundation (NSF) EaSM2 grant OCE-1243015. NCAR is sponsored by the NSF under Cooperative Agreement 1852977. Computing resources were provided by the Climate Simulation Laboratory at NCAR's Computational and Information Systems Laboratory, sponsored by the NSF. The NSF and DOE BER RGCM support the CESM project. This is UW/CICOES contribution 2020-1134 and PMEL contribution 5238.

References

Biastoch, A., Böning, C. W., Getzlaff, J., Molines, J. M., & Madec, G. (2008). Causes of interannual–decadal variability in the meridional overturning circulation of the midlatitude North Atlantic Ocean. *Journal of Climate*, *21*(24), 6599–6615. https://doi.org/10.1175/2008jcli2404.1

Bretherton, C. S., Smith, C., & Wallace, J. M. (1992). An intercomparison of methods for finding coupled patterns in climate data. *Journal of Climate*, *5*(6), 541–560. https://doi.org/10.1175/1520-0442(1992)005<0541:aiomff>2.0.co;2

Buckley, M. W., Ferreira, D., Campin, J. M., Marshall, J., & Tulloch, R. (2012). On the relationship between decadal buoyancy anomalies and variability of the Atlantic meridional overturning circulation. *Journal of Climate*, *25*(23), 8009–8030. https://doi.org/10.1175/jcli-d-11-00505.1

Buckley, M. W., & Marshall, J. (2016). Observations, inferences, and mechanisms of the Atlantic Meridional Overturning Circulation: A review. *Reviews of Geophysics*, *54*(1), 5–63. https://doi.org/10.1002/2015rg000493

Czaja, A., & Frankignoul, C. (1999). Influence of the North Atlantic SST on the atmospheric circulation. *Geophysical Research Letters*, *26*(19), 2969–2972. https://doi.org/10.1029/1999GL900613

Danabasoglu, G. (2008). On multidecadal variability of the Atlantic meridional overturning circulation in the Community Climate System Model version 3. *Journal of Climate*, *21*(21), 5524–5544. https://doi.org/10.1175/2008jcli2019.1

Danabasoglu, G., Yeager, S. G., Kwon, Y. O., Tribbia, J. J., Phillips, A. S., & Hurrell, J. W. (2012). Variability of the Atlantic meridional overturning circulation in CCSM4. *Journal of Climate*, *25*(15), 5153–5172. https://doi.org/10.1175/jcli-d-11-00463.1

Delworth, T. L., Manabe, S., & Stouffer, R. J. (1993). Interdecadal variations of the thermohaline circulation in a coupled ocean-atmosphere model. *Journal of Climate*, *6*(11), 1993–2011. https://doi.org/10.1175/1520-0442(1993)006<1993:ivottc>2.0.co;2

Delworth, T. L., & Zeng, F. (2016). The impact of the North Atlantic Oscillation on climate through its influence on the Atlantic meridional overturning circulation. *Journal of Climate*, *29*(3), 941–962. https://doi.org/10.1175/jcli-d-15-0396.1

Deshayes, J., & Frankignoul, C. F. (2008). Simulated variability of the circulation in the North Atlantic from 1953 to 2003. *Journal of Climate*, *21*, 4919–4933. https://doi.org/10.1175/2008jcli1882.1

Dong, B., & Sutton, R. T. (2005). Mechanism of interdecadal thermohaline circulation variability in a coupled ocean–atmosphere GCM. *Journal of Climate*, *18*(8), 1117–1135. https://doi.org/10.1175/jcli3328.1

Ebisuzaki, W. (1997). A method to estimate the statistical significance of a correlation when the data are serially correlated. *Journal of Climate*, *10*(9), 2147–2153. https://doi.org/10.1175/1520-0442(1997)010<2147:amtets>2.0.co;2

Gastineau, G., & Frankignoul, C. (2012). Cold-season atmospheric response to the natural variability of the Atlantic meridional overturning circulation. *Climate Dynamics*, *39*, 37–57. https://doi.org/10.1007/s00382-011-1109-y

Griffies, S. M., & Tziperman, E. (1995). A linear thermohaline oscillator driven by stochastic atmospheric forcing. *Journal of Climate*, *8*(10), 2440–2453. https://doi.org/10.1175/1520-0442(1995)008<2440:altodb>2.0.co;2

Häkkinen, S. (1999). Variability of the simulated meridional heat transport in the North Atlantic for the period 1951–1993. *Journal of Geophysical Research*, *104*(C5), 10991–11007. https://doi.org/10.1029/1999jc900034

Huang, N. E., Shen, Z., Long, S. R., Wu, M. C., Shih, H. H., Zheng, Q., et al. (1998). The empirical mode decomposition and the Hilbert spectrum for nonlinear and non-stationary time series analysis. *Proceedings of the Royal Society of London. Series A: Mathematical, Physical and Engineering Sciences*, *454*(1971), 903–995. https://doi.org/10.1098/rspa.1998.0193

Kay, J. E., & Deser, C. (2016). *The Community Earth System Model (CESM) large ensemble project*. UCAR/NCAR Climate Data Gateway. https://doi.org/10.5065/d6j101d1

Kay, J. E., Deser, C., Phillips, A., Mai, A., Hannay, C., Strand, G., et al. (2015). The Community Earth System Model (CESM) large ensemble project: A community resource for studying climate change in the presence of internal climate variability. *Bulletin of the American Meteorological Society*, *96*(8), 1333–1349. https://doi.org/10.1175/bams-d-13-00255.1

Kim, W. M., Yeager, S., & Danabasoglu, G. (2020). Atlantic multidecadal variability and associated climate impacts initiated by ocean thermohaline dynamics. *Journal of Climate*, *33*(4), 1317–1334. https://doi.org/10.1175/jcli-d-19-0530.1

Kwon, Y. O., & Frankignoul, C. (2012). Stochastically-driven multidecadal variability of the Atlantic meridional overturning circulation in CCSM3. *Climate Dynamics*, *38*(5–6), 859–876. https://doi.org/10.1007/s00382-011-1040-2

Kwon, Y. O., & Frankignoul, C. (2014). Mechanisms of multidecadal Atlantic meridional overturning circulation variability diagnosed in depth versus density space. *Journal of Climate*, *27*(24), 9359–9376. https://doi.org/10.1175/jcli-d-14-00228.1

Larson, S. M., Buckley, M. W., & Clement, A. C. (2020). Extracting the Buoyancy-driven Atlantic meridional overturning circulation. *Journal of Climate*, *33*(11), 4697–4714. https://doi.org/10.1175/jcli-d-19-0590.1

Tandon, N. F., & Kushner, P. J. (2015). Does external forcing interfere with the AMOC's influence on North Atlantic sea surface temperature? *Journal of Climate*, *28*(16), 6309–6323. https://doi.org/10.1175/jcli-d-14-00664.1

Wu, Z., & Huang, N. E. (2009). Ensemble empirical mode decomposition: A noise-assisted data analysis method. *Advances in Adaptive Data Analysis*, *1*(01), 1–41. https://doi.org/10.1142/s1793536909000047

Zhang, J., & Zhang, R. (2015). On the evolution of Atlantic meridional overturning circulation fingerprint and implications for decadal predictability in the North Atlantic. *Geophysical Research Letters*, *42*(13), 5419–5426. https://doi.org/10.1002/2015gl064596

Zhang, R. (2008). Coherent surface-subsurface fingerprint of the Atlantic meridional overturning circulation. *Geophysical Research Letters*, *35*(20). https://doi.org/10.1029/2008gl035463